Journal of
Polymer & Composites
https://journals.stmjournals.com/jopc

ISSN: 2321-2810 (Online)
ISSN: 2321-8525 (Print)
Volume 13, Regular Issue 5, 2025
DOI (Journal): 10.37591/JoPC

Research JoPC

Facile Synthesis and Characterization of Cd^{2+} Doped $NiAl_2O_4$ Nanoparticles for Advanced Polymer Composite Integration

S. Dhanabalan[1], R. T. Karunakaran[2,*], S. Prabahar[3], S. Nithya[4], S. Yuvaraj[5], R. Kiruthika[6]

Abstract

$Ni_{1-x}Cd_xAl_2O_4$, where $0 \leq x \leq 0.5$, was successfully synthesized using the chemical co-precipitation technique, a scalable and cost-effective route suitable for composite material applications. X-ray diffraction (XRD) analysis revealed a crystalline cubic spinel structure for the resulting nanoparticles, with determined crystallite sizes ranging from 36 to 12 nm for $NiAl_2O_4$ and Cd-doped $NiAl_2O_4$. The respective band gaps for the materials were found to be 3.51 and 4.18 eV. Infrared (IR) studies confirmed the bond formation of the synthesized nanoparticles, with notable IR bands at 495 cm^{-1} corresponding to octahedral-metal (Ni-O) stretching and a band at 563 cm^{-1} corresponding to tetrahedral metal stretching (Al-O), indicating the production of cadmium-doped nickel aluminate nanoparticles. The synthesized nanoparticles displayed ferromagnetic behavior, and magnetic characteristics such as remanent magnetization (M_r), coercivity (H_c), and saturation magnetization (M_s) were determined through M-H loop analysis. Nonlinear optical properties, including the nonlinear index of refraction (10^{-8} cm^2/W), nonlinear absorption coefficient (10^{-4} cm/W), and the 3^{rd} order nonlinear susceptibility (10^{-6} esu), were determined through Z-scan experiments. The materials also displayed effective optical limiting behavior, underscoring their potential as active fillers in polymer-based composite systems for photonic protection, smart coatings, and optoelectronic devices. The findings suggest that Cd-doped $NiAl_2O_4$ nanoparticles are promising candidates for the development of multifunctional polymer nanocomposites with tailored optical and magnetic functionalities.

Keywords: Cd doped $NiAl_2O_4$ nanoparticles; spinel structure; polymer-compatible fillers; optical limiting; functional composites

***Author for Correspondence**
R. T. Karunakaran
E-mail: drkarunakaranrt@gmail.com

[1] Assistant Professor, Department of Physics, Sri Ranganathar Institute of Engineering and Technology, Coimbatore, Tamil Nadu, India
[2,3]Associate Professor, Department of Physics, Government Arts College, Udumalpet, Tiruppur, Tamil Nadu, India.
[4]Assistant Professor, Department of Physics, Vel Tech Rangarajan Dr. Sagunthala R&D Institute of Science and Technology, Avadi, Chennai, Tamil Nadu, India
[5]Associate Professor, Department of Physics, Vel Tech Rangarajan Dr. Sagunthala R&D Institute of Science and Technology, Avadi, Chennai, Tamil Nadu, India
[6]Assistant Professor, Department of Agricultural Engineering, Nehru Institute of Technology, Coimbatore, Tamil Nadu, India

Received Date: July 10, 2025
Accepted Date: July 17, 2025
Published Date: August 07, 2025

Citation: S. Dhanabalan, R. T. Karunakaran, S. Prabahar, S. Nithya, S. Yuvaraj, R. Kiruthika. Facile synthesis and characterization of Cd^{2+} Doped $NiAl_2O_4$ Nanoparticles for Advanced Polymer Composite Integration. Journal of Polymer & Composites. 2025; 13(Regular Issue 5): 59–72p.

INTRODUCTION

In recent years, the emergence of advanced nanomaterials has opened new pathways for developing high-performance polymer composites tailored for multifunctional applications [1]. Among the various types of nanomaterials, metal oxide-based spinel nanoparticles have garnered considerable attention due to their remarkable structural, magnetic, and optical characteristics. When combined with polymers, these nanoparticles contribute to the development of hybrid materials with enhanced thermal stability, mechanical strength, and novel optical functionalities especially nonlinear optical (NLO) behavior. Such hybrid systems are in high demand in the fields of optoelectronics, photonics, electromagnetic shielding, and protective optical devices, such as optical limiters.

Laser technology has witnessed rapid advancements and wide-ranging applications in fields such as telecommunications, defense, and medical diagnostics. However, the increased use of high-intensity lasers has also raised concerns regarding the protection of sensitive optical sensors and human vision. As a result, the development of optical limiting devices has become a major focus in photonic research. These devices allow light to pass through under normal conditions but attenuate it when the input intensity exceeds a certain threshold. The materials used in such devices must exhibit high linear transmittance, low threshold nonlinear response, and broadband stability. Nonlinear optical materials that can undergo reverse saturable absorption (RSA), two-photon absorption (TPA), and nonlinear refraction (NLR) have emerged as suitable candidates for these applications [2, 3].

While organic molecules such as phthalocyanines and porphyrins have been extensively studied for NLO applications, they often suffer from limitations like low photochemical stability and significant absorption in the visible region, making them less suitable for real-world optical protection. In contrast, inorganic nanomaterials, especially those with spinel structures, have demonstrated superior stability, tunable properties, and better compatibility with polymeric matrices, making them ideal for polymer-based nonlinear optical composites [4–6]. In the past decade, semiconductors have assumed a vital place in nanoscience and nanotechnology, owing to their remarkable optical, structural, electrical and magnetic properties. Their applications span a wide range including magnetic storage, energy storage devices, resistive memory devices, piezoelectricity and photocatalytic degradation. Among the various materials investigated, metal oxide semiconductors, studied in numerous research endeavors, stand out as essential materials in this field [7-11].

A commonly observed structural configuration is the cubic spinel structure and is represented by the general formula AB_2O_4. Here, 'A' indicates elements such as Cd^{2+}, Co^{2+}, Ni^{2+}, Mn^{2+}, occupying tetrahedral A sites, while 'B' indicates elements like Al^{3+}, Fe^{3+}, occupying octahedral B sites. This structural arrangement exhibits distinctive physical and magnetic characteristics, particularly when alterations are made to the divalent cation [12]. Recent studies have identified Ni-Cd aluminates as magnetic materials with unique characteristics, showcasing their versatility across various applications. These aluminates play a crucial role in applications such as power transformers, read/write heads for high-speed digital tapes, microwave-equipped devices and rod antennae [13]. Moreover, these materials have proven effectiveness in gas sensing applications [14, 15]. Importantly, such doped spinel nanoparticles, when embedded into polymer matrices like PMMA, PVDF, or epoxy resins, can significantly enhance the composite's performance due to improved dispersion, interfacial bonding, and the inherent multifunctionality of the fillers. The integration of magnetic and NLO-active nanofillers in polymers paves the way for smart materials with dual functionality ideal for optoelectronic switching, tunable optics, and electromagnetic shielding [16–18]. To this end, the proper synthesis and control of nanoparticle characteristics such as particle size, phase purity, and surface morphology become critical for ensuring their effectiveness in polymer composites.

The nanoparticles of $Cd:NiAl_2O_4$ exhibit a mixed spinel structure, where octahedral sites are occupied by Ni^{2+}, Cd^{+2} and Al^{3+} ions, and tetrahedral sites house Cd^{+2}, Ni^{2+} and Al^{3+} ions within the lattice. Notably, the preparation of aluminates at lower temperatures, coupled with nanoscale particle sizes, introduces variations in the distribution of ions across octahedral and tetrahedral sites. To produce cadmium-doped nickel aluminates nanoparticles, various techniques like sol-gel, microwave-assisted combustion, solvothermal, hydrothermal and ball milling have been commonly employed [19-22]. However, these methods often come with drawbacks such as complexity, synthesis difficulty, time-consuming processes, low yields and high costs. In response to these challenges, the chemical co-precipitation method is adopted for the synthesis of cadmium-doped nickel aluminate nanoparticles. This method enables better control over particle size, morphology and surface area, while being cost-effective, energy-efficient and easily scalable for large-scale production. Cadmium-doped nickel aluminates synthesized via the chemical co-precipitation technique offer several advantages, including enhanced structural uniformity and improved crystallinity. The doping of Cd^{2+} ions allow for tuning of optical properties, such as band gap reduction and photoluminescence enhancement, making them suitable for optoelectronic applications.

In this particular work, the chemical co-precipitation method is employed to create nanoparticles of $Ni_{1-x}Cd_xAl_2O_4$ (where $0 \leq x \leq 0.5$). The choice of dopants, even in slight variations lead to significant differences in textural, structural, morphological, vibrational, optical and magnetic properties of the synthesized nanoparticles. The study further investigates the phase, vibrational, morphological, magnetic, and optical characteristics of the synthesized nanoparticles using a range of characterization methods. The ultimate goal is to evaluate the potential of these nanoparticles as functional nanofillers for polymer-based nanocomposites with applications in optical limiting, magnetic data storage, gas sensing, and smart device fabrication. By understanding the relationship between cationic substitution and functional properties, and by employing a synthesis method suitable for large-scale production, this work aims to contribute to the development of next-generation magneto-optical polymer composites. These composites are expected to meet the growing demand for multifunctional materials that can operate under extreme conditions while offering tunable magnetic and optical performance. Moreover, altering the band gap and enhancing electrical conductivity can contribute to increased charge carrier mobility, reduced interfacial resistance, and improved signal responsiveness in sensor platforms. In polymer-based sensors, such nanocomposites may also offer enhanced sensitivity, faster response times, and better thermal stability. Overall, these tailored nanoscale features open up promising possibilities for the development of advanced materials for flexible electronics, EMI shielding, wearable sensors, and next-generation smart devices [23-28].

EXPERIMENTAL WORK

Synthesis Procedure

In the chemical co-precipitation approach employed for generating nanosized $Ni_{1-x}Cd_xAl_2O_4$ samples, the following steps were undertaken: Analytical reagent (AR) grade nickel chloride, aluminum chloride and cadmium chloride were used as precursors at a concentration of 0.1M. The choice of precursors is crucial in determining the composition and properties of the synthesized nanoparticles. A homogeneous solution was achieved by simultaneously applying a 1:2 ratio of Ni/NiCd:Al, followed by stirring. This step ensures the proper mixing of the metal ions in the desired stoichiometric ratio. And 3M sodium hydroxide solution was gradually added drop wise to the blended solution. This process led to the formation of a precipitate at pH 12. The control of pH is a critical parameter influencing the morphology, form and the size of the crystallites. The product obtained from the precipitation step was completely dissolved at 120°C for duration of thirty minutes. Temperature plays a significant role in achieving samples with a crystalline nature. The precipitate produced was repeatedly washed with ethanol and double-distilled water. This washing step is essential for removing impurities and unreacted precursors from the synthesized samples. Using the same process, various concentrations of $Ni_{1-x}Cd_xAl_2O_4$ (x = 0, 0.10, 0.30, and 0.50) were synthesized. This variation in composition allows for the exploration of different material properties and characteristics. The chemical co-precipitation method offers advantages in terms of simplicity, scalability and the potential to control the synthesis parameters for tailoring the properties of the resulting nanoparticles.

Characterization

The $NiAl_2O_4$ nanoparticles were involved to X-ray Powder Diffractometry. Rigaku Ultima III model X-ray powder diffractometer was employed, utilizing CuKα radiation with a wavelength (λ) of 1.5406 Å. The diffractometer covered the 2θ range between 20° and 80°, providing information on the phase and crystal structure of $NiAl_2O_4$ nanoparticles. Morphological and elemental analyses were performed using Scanning Electron Microscopy (FEI Quanta FEG 200 model SEM). This technique offers high-resolution imaging of the surface morphology of the nanoparticles. The band gap value of $NiAl_2O_4$ nanoparticles was determined from the diffuse reflectance spectrum. This measurement was conducted using a Perkin Elmer spectrophotometer (Thermo Scientific Evolution 220) in the wavelength range from 200 nm to 800 nm. An FTIR spectrum was acquired using a Perkin Elmer spectrophotometer (Spectrum RX1). FTIR is an analytical technique for analyzing vibrational modes in the infrared region, providing insights into the chemical composition and bonding in the material. Room temperature magnetic properties of the nanoparticles were studied using Lake Shore Model 7404 vibration sample magnetometer. This technique helps in understanding the magnetic behavior of the material. The

Holmarc's Z-Scan System (Model No: HO-ED-LOE-03) was utilized to measure the third-order nonlinear parameters. This involves studying the material's response to intense laser irradiation, providing information about nonlinear optical properties. The combination of these techniques leads to a comprehensive understanding of the structural, morphological, elemental, optical, and magnetic properties of $NiAl_2O_4$ nanoparticles. The diverse set of characterization methods ensures a thorough investigation of the material's features and its potentiality for various technological applications.

RESULTS AND DISCUSSION

Structure and Phase Analysis

The X-ray diffraction (XRD) pattern presented in Fig. 1 provides a detailed phase analysis of both the $NiAl_2O_4$ and Cd:$NiAl_2O_4$ nanoparticles in their as-synthesized state. The diffraction peaks clearly indicate the polycrystalline nature of the synthesized samples. Peaks with diffracted 2θ values viz., 31.40˚, 37.01˚, 44.99˚, 55.97˚, 59.66˚ and 65.53˚ correspond to the hkl plane of (220), (311), (400), (422), (511) and (440) of the synthesized $NiAl_2O_4$ nanoparticles. The identified diffraction peaks well-matched with JCPDS card number 10-0339, confirming the Fd-3m space group with the cubic spinel structure [29]. There is no secondary peak observed and results indicate the phase purity of the synthesized $NiAl_2O_4$ nanoparticles.

The Debye Scherrer equation is a fundamental formula used to determine the average crystallite size (L) of nanoparticles based on X-ray diffraction data. The equation is given

$$L = \frac{K\lambda}{BCOS\theta} \quad (1)$$

where L is the average crystallite size, K is the shape factor (usually taken as 0.89), λ is the X-ray wavelength, β is the full width at half maximum (FWHM) of the diffraction peak, θ is the diffraction angle. The mean crystallite size of Cd:$NiAl_2O_4$ and $NiAl_2O_4$ nanoparticles were determined to be in the range between 12 and 36 nm with respect to the diffraction peak (311). This information is valuable in understanding the size of the crystalline domains in the synthesized nanoparticles. The smaller crystallite size for Cd:$NiAl_2O_4$ suggests that the introduction of cadmium (Cd) has an impact on reducing the average crystallite size compared to the cadmium-free $NiAl_2O_4$.

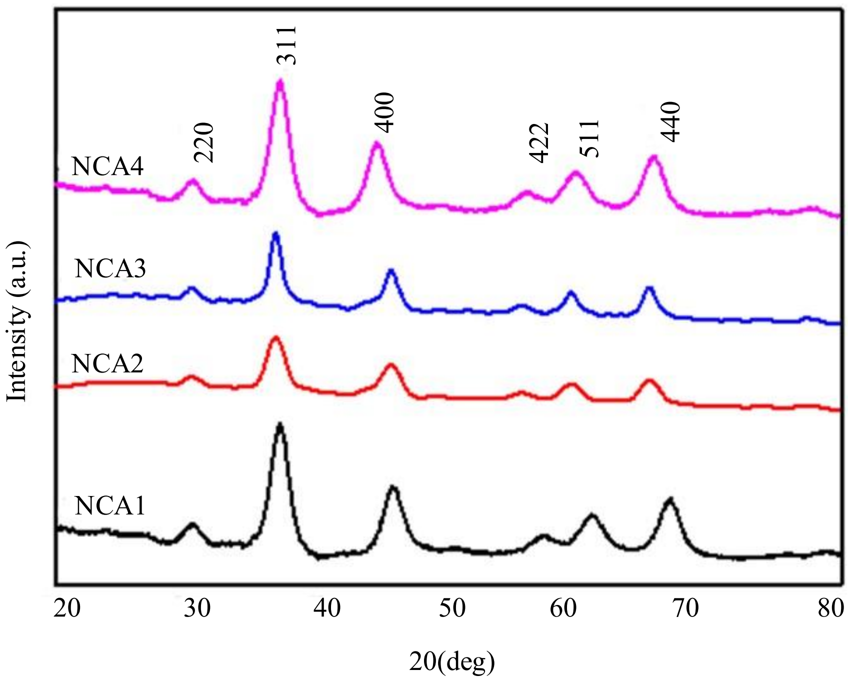

Figure 1. Powder X-Ray diffraction pattern of $Ni_{1-x}Cd_xAl_2O_4$ ($0 \leq x \leq 0.5$) nanoparticles.

Table 1. Crystallite size, lattice parameter and energy gap of $Ni_{1-x}Cd_xAl_2O_4$ ($0 \leq x \leq 0.5$) nanoparticles.

Sample name	Sample code	Crystallite size, L (nm)	Lattice parameter, a (Å)	Energy gap (eV)
$NiAl_2O_4$	NA1	36	8.0472	3.51
$Ni_{0.9}Cd_{0.1}Al_2O_4$	NCA2	28	8.0470	3.79
$Ni_{0.7}Cd_{0.3}Al_2O_4$	NCA3	18	8.0469	3.94
$Ni_{0.5}Cd_{0.5}Al_2O_4$	NCA4	12	8.0462	4.18

Equation (2) is used to derive the lattice parameter (a) of the cubic spinel structure for both $NiAl_2O_4$ and $Cd{:}NiAl_2O_4$ nanoparticles. The equation is given by:

$$a = d_{hkl}\sqrt{h^2 + k^2 + l^2} \quad (2)$$

where a is the lattice parameter, d_{hkl} is the inter-planar distance of (h k l) planes. The lattice parameter values of $Cd{:}NiAl_2O_4$ and $NiAl_2O_4$ nanoparticles were found to be in between 8.0462 Å and 8.0472 Å. These values are consistent with the previously reported value of 8.0480 Å [30]. The lattice parameter is a measure of the size of the unit cell in the crystal lattice. In this case, the observed decrease in the lattice parameter when Cd cations (ionic radius of 0.97 Å) are substituted for Ni cations (ionic radius of 0.69 Å) aligns with Vegard's law.

Vegard's law describes the linear relationship between the lattice parameter and the composition of solid solutions, indicating a slight decrease in the crystal size due to the substitution of Cd cations for Ni cations. This observation provides insights into the structural changes induced by the presence of cadmium in the spinel structure. Table 1 indicates that the crystallite size and lattice parameters decrease with increasing Cd^{2+} ions content (x), highlighting the impact of cadmium doping on the structural properties of the synthesized nanoparticles [31,32].

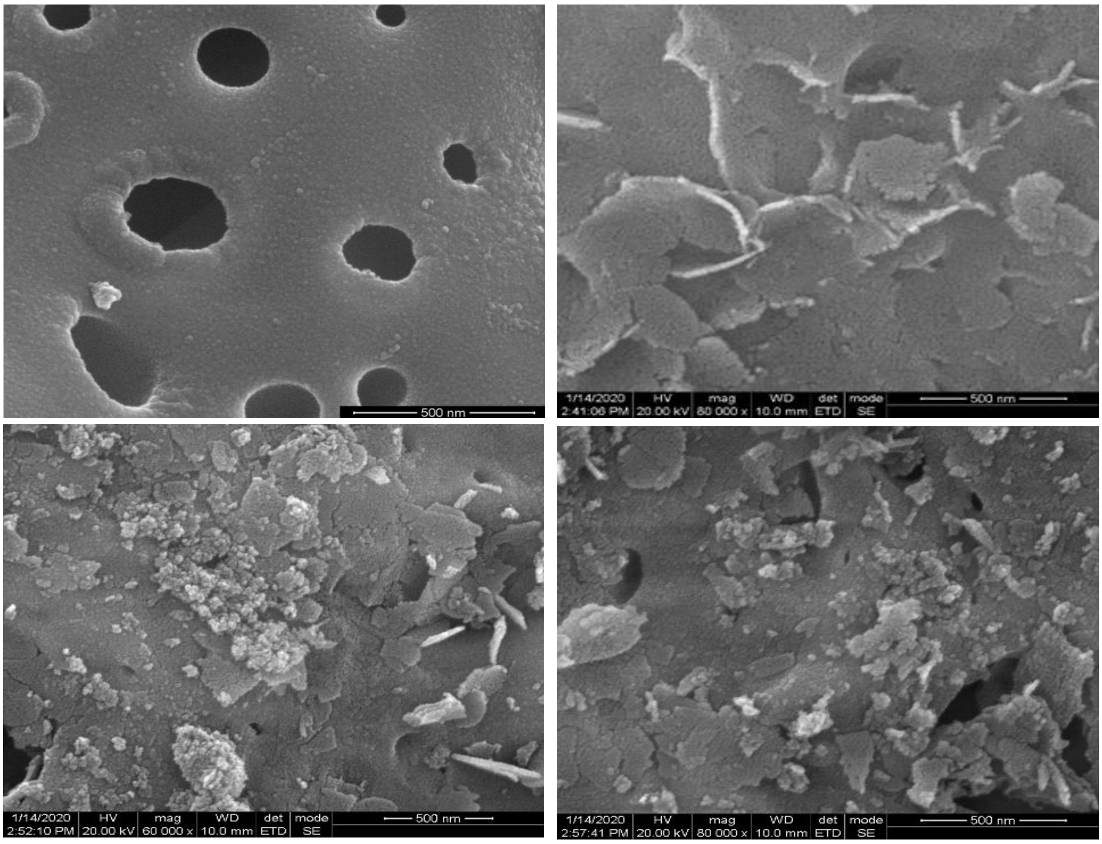

Figure 2. HR-SEM images of (a) $NiAl_2O_4$ (b) $Ni_{0.9}Cd_{0.1}Al_2O_4$ (c) $Ni_{0.7}Cd_{0.3}Al_2O_4$ and (d) $Ni_{0.5}Cd_{0.5}Al_2O_4$ nanoparticles.

Surface Morphology

The surface morphology of the synthesized Cd:$NiAl_2O_4$ and $NiAl_2O_4$ nanoparticles, as illustrated in Figure 2, reveals significant insights into their structural characteristics relevant to composite material applications. Scanning Electron Microscopy (SEM) images indicate that the particles exhibit agglomeration and coalescence, which is commonly observed in nanoscale systems due to high surface energy. The formation of interconnected clusters and the presence of porous structures suggest the existence of internal voids and surface roughness, which could enhance interfacial interaction when incorporated into polymer matrices. SEM images show that Cd^{2+} doping alters the surface morphology, leading to more refined and homogeneously distributed nanoparticles, which may improve interfacial compatibility in polymer composites. Moreover, the nanoparticles tend to adopt a quasi-spherical morphology, attributed to the reduced surface energy and controlled kinetics during the co-precipitation synthesis process [33]. These features are advantageous for uniform dispersion and enhanced load transfer within polymer-based composites.

Bandgap Analysis

The bandgap of the synthesized materials was calculated from the results of UV-Visible spectroscopy. Equation (3) indicate the Kubelka-Munk function F(R) giving absorption co-efficient from the diffused reflectance spectrum.

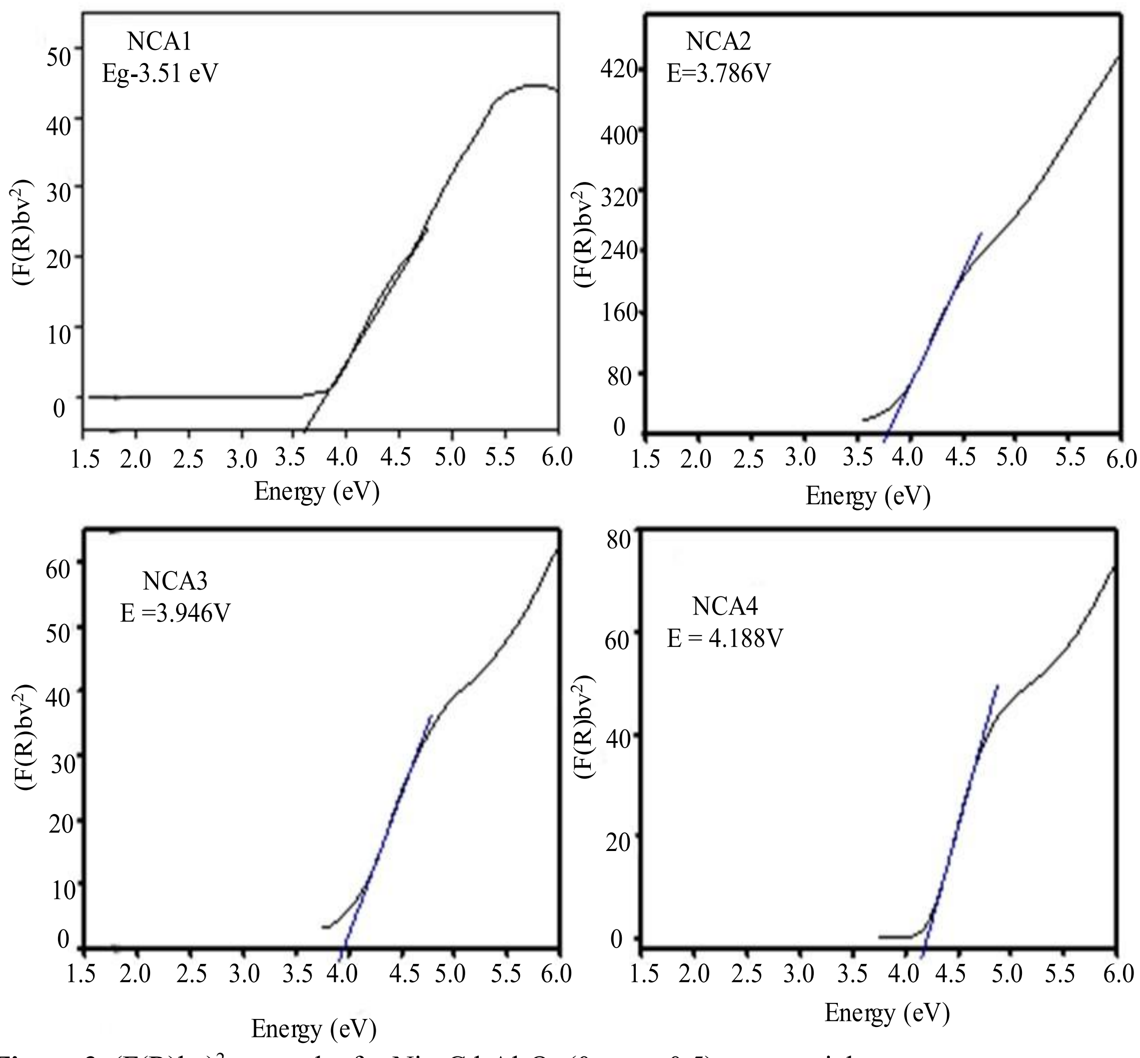

Figure 3. $(F(R)h\upsilon)^2$ versus $h\upsilon$ for $Ni_{1-x}Cd_xAl_2O_4$ ($0 \le x \le 0.5$) nanoparticles.

$$\alpha = F(R) = \frac{(1-R)^2}{2R} \tag{3}$$

Tauc relation is commonly used to estimate the bandgap of a material from its optical absorption spectrum and it is typically expressed as equation (4):

$$\alpha h\nu = A(h\nu - Eg)^n \tag{4}$$

where α is the absorption coefficient, hν is the energy of the incident photon, A is a constant, E_g is the bandgap energy, n is an exponent that depends on the nature of the transition (for indirect bandgap n = 1/2).The Tauc plot for Cd:$NiAl_2O_4$ and $NiAl_2O_4$ nanoparticles allows to determine the energy band gaps through extrapolation of the linear portion of the graph which is shown in Fig.3. The optical band gap energies of the synthesized samples NA1, NCA1, NCA2, and NCA3 were determined to be 3.51, 3.79, 3.94, and 4.18 eV, respectively, in contrast to the reported value of 2.2 eV for bulk $NiAl_2O_4$ [34-36]. The progressive increase in band gap values with Cd^{2+} doping can be attributed to several factors, including quantum confinement effects, reduced crystallite size, and the presence of lattice defects. These nanoscale phenomena significantly alter the electronic structure, leading to modified optical absorption characteristics [37]. Such tunable band gap behavior is particularly advantageous for tailoring the optical transparency and photonic performance of polymer-based nanocomposites, where controlled light-matter interaction is crucial for applications in UV-blocking coatings, optical filters, and photoprotective materials.

FT-IR Spectra

The FTIR analysis provides a comprehensive understanding of the molecular structure, bonding and functional groups present in the synthesized $Ni_{1-x}Cd_xAl_2O_4$ nanoparticles.

Figure 4. shows the FTIR spectra of $Ni_{1-x}Cd_xAl_2O_4$ polycrystalline aluminates obtained in the mid-IR region (400 - 4000 cm^{-1}). The peaks observed between 400 and 1000 cm^{-1} remain the fingerprint of metal ion vibrations in the crystal lattice. Absorption peaks at 563 and 495 cm^{-1} are attributed to stretching vibrations between transition metal and oxygen ions [38]. These peaks confirm the synthesis of cubic spinel aluminates. Chemical bonds between trivalent iron and oxygen ions ($Al^{3+} \leftrightarrow O^{2-}$) are located at the B-octahedral site. Divalent nickel/cadmium and oxygen bonds ($M^{2+} \leftrightarrow O^{2-}$) are located at the A-tetrahedral site. The frequency of the stretching band shifts to a higher wavenumber as the concentration of doping (Ni/Cd) increases [39]. Stretching and bending vibrations at 1447, 1565, 1610, 3436, and 1532 cm^{-1} confirm the surface adsorption of OH groups in aluminate nanoparticles [40]. Stretching vibrations of organic molecules such as -CH/-CO chemical molecules located at 2855 and 2926 cm^{-1} indicate the presence of water in the samples [41].

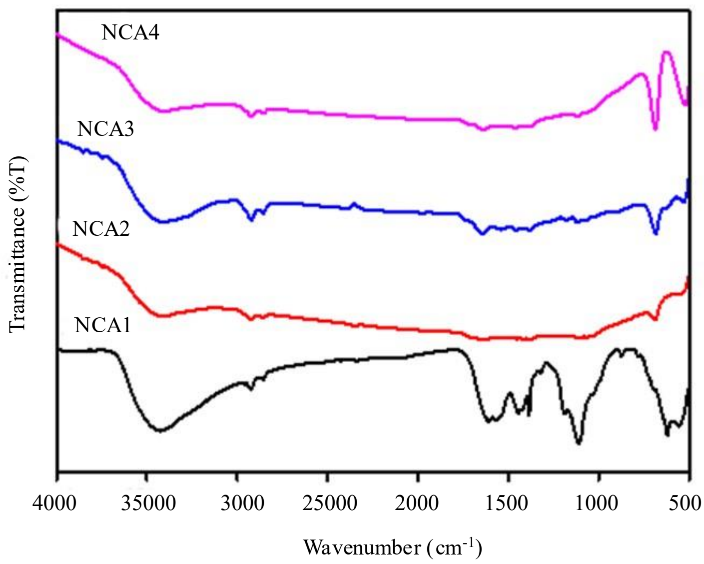

Figure 4. FT-IR spectra of $Ni_{1-x}Cd_xAl_2O_4$ ($0 \le x \le 0.5$) nanoparticles.

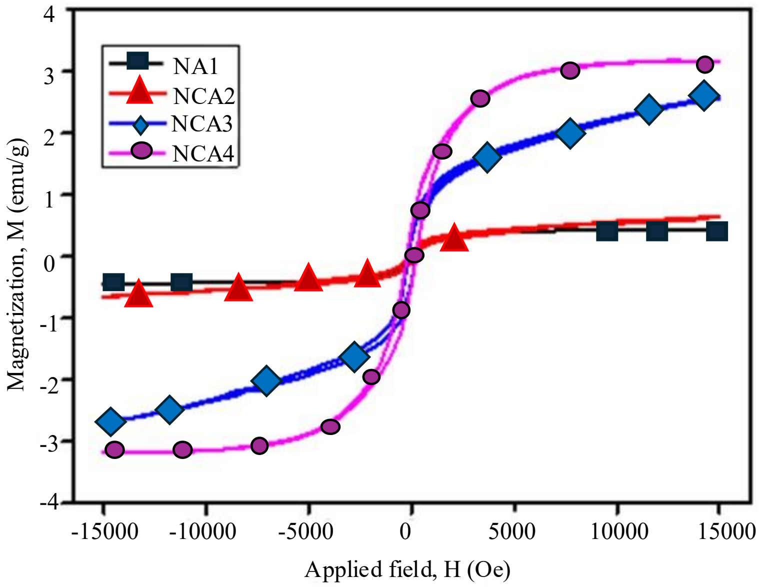

Figure 5. Hysteresis loop of $Ni_{1-x}Cd_xAl_2O_4$ ($0 \leq x \leq 0.5$) nanoparticles.

Table 2. Coercivity, remanent magnetization, saturation magnetization values of $Ni_{1-x}Cd_xAl_2O_4$ ($0 \leq x \leq 0.5$) nanoparticles.

Sample name	Sample code	H_c, (O_e)	M_r (emu/g)	M_s (emu/g)
$NiAl_2O_4$	NA1	189.16	6.23	0.51
$Ni_{0.9}Cd_{0.1}Al_2O_4$	NCA2	197.74	5.72	1.76
$Ni_{0.7}Cd_{0.3}Al_2O_4$	NCA3	213.53	5.14	2.97
$Ni_{0.5}Cd_{0.5}Al_2O_4$	NCA4	235.12	4.78	3.81

Magnetization Study

The investigation of the magnetic properties of Cd:$NiAl_2O_4$ and $NiAl_2O_4$ nanoparticles was carried out at 300 K under a magnetic field (-15 kOe to +15 kOe). Fig.5. reveals the behavior of the samples under investigation and the values of remanence magnetization (M_r), coercivity (H_c) and saturation magnetization (M_s) obtained from the hysteresis loop as detailed in Table.2. The nanoparticles possessing a standard spinel composition with divalent (Ni^{2+}/Cd^{2+}) and trivalent (Al^{3+}) metal ions occupying tetrahedral and octahedral positions, exhibit a ferromagnetic nature, especially for $NiAl_2O_4$.

Coercivity is maximum for NCA4, i.e., 235.12 Oe, while it is 189.16 Oe for pure $NiAl_2O_4$. These values indicate the influence of high anisotropy and cationic redistribution on the magnetic behavior [42]. Notable variations in remanence magnetization (M_r) values are observed for cadmium-doped nickel aluminates nanoparticles. The M_r values decrease with increasing cadmium doping ($x=0.5 < 0.3 < 0.1 < 0.0$) with the values of 4.78 emu/g, 5.14 emu/g, 4.78 emu/g and 6.23 emu/g respectively, and the emphasis is the dependence of M_r on the crystallite size and shape of nickel aluminates [43,44].

Saturation magnetization (M_s) values for $NiAl_2O_4$ and Cd:$NiAl_2O_4$ nanoparticles present in the range of (~ 0.51 – 3.81 emu/g), as calculated from the hysteresis loop. These characteristics suggest that Cd-doped $NiAl_2O_4$ nanoparticles are promising candidates as magnetically responsive fillers in polymer matrix composites, offering potential applications in magnetic sensing, electromagnetic shielding, and smart actuating systems.

Nonlinear Optical Studies (Z-scan)

Z-scan techniques were used to investigate in the present work the influence of Cd doping in Ni aluminate nanoparticles towards nonlinear properties. The obtained Z-scan patterns as shown in Figure

6 represent the normalized transmittance versus the location of the sample in nm. This study provides the information of nonlinear absorption and refraction details in both the open-aperture and closed-aperture modes. The division approach allows isolating and distinguishing the nonlinear absorption and refraction effects [45]

Evaluation of Nonlinear Absorption

Figure 6(b) indicate the open aperture Z-scan graph showing saturable absorption characteristics of the synthesized material. Saturable absorption is a nonlinear optical phenomenon in which the materials absorption decreases as the intensity of incident light increases.

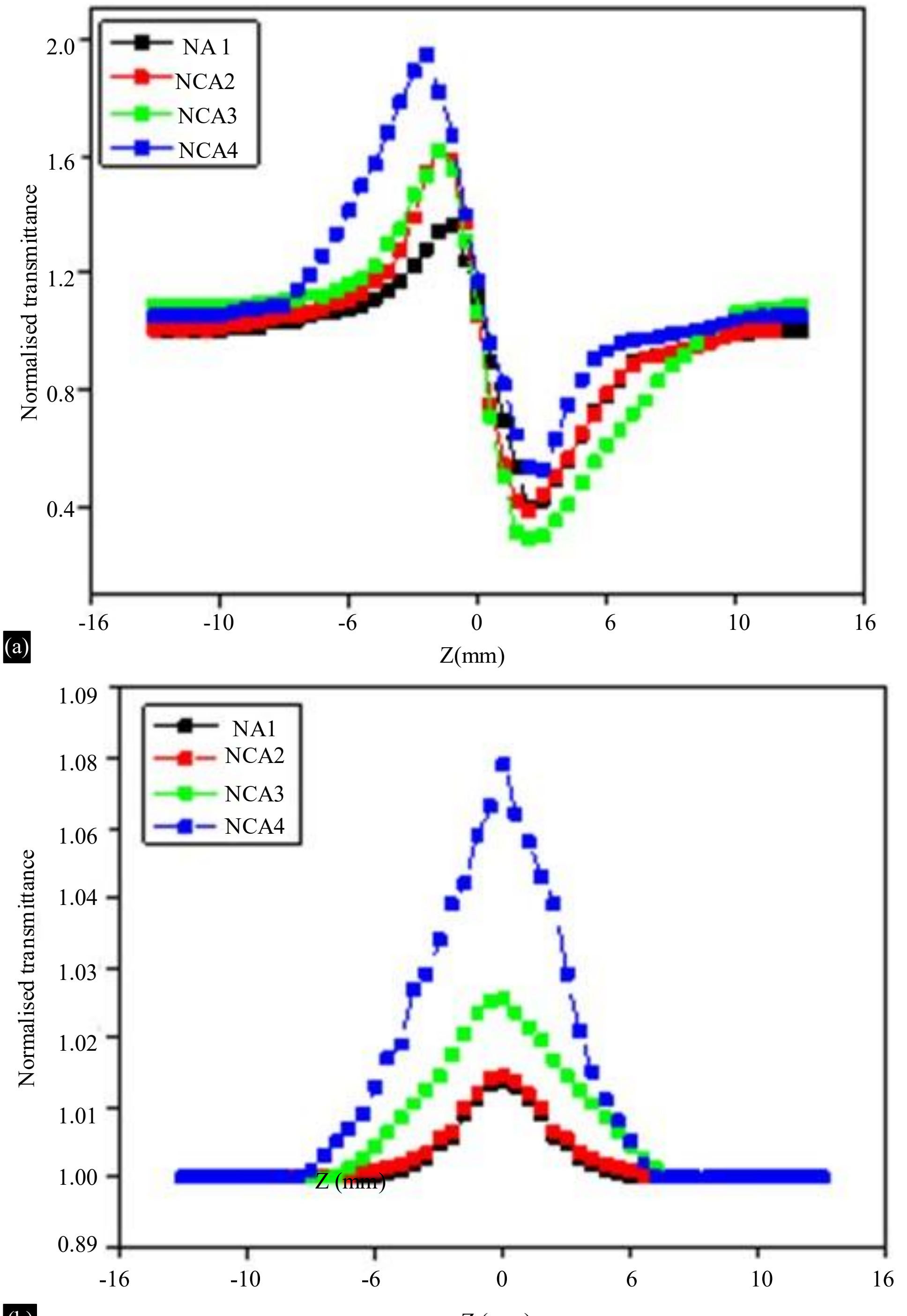

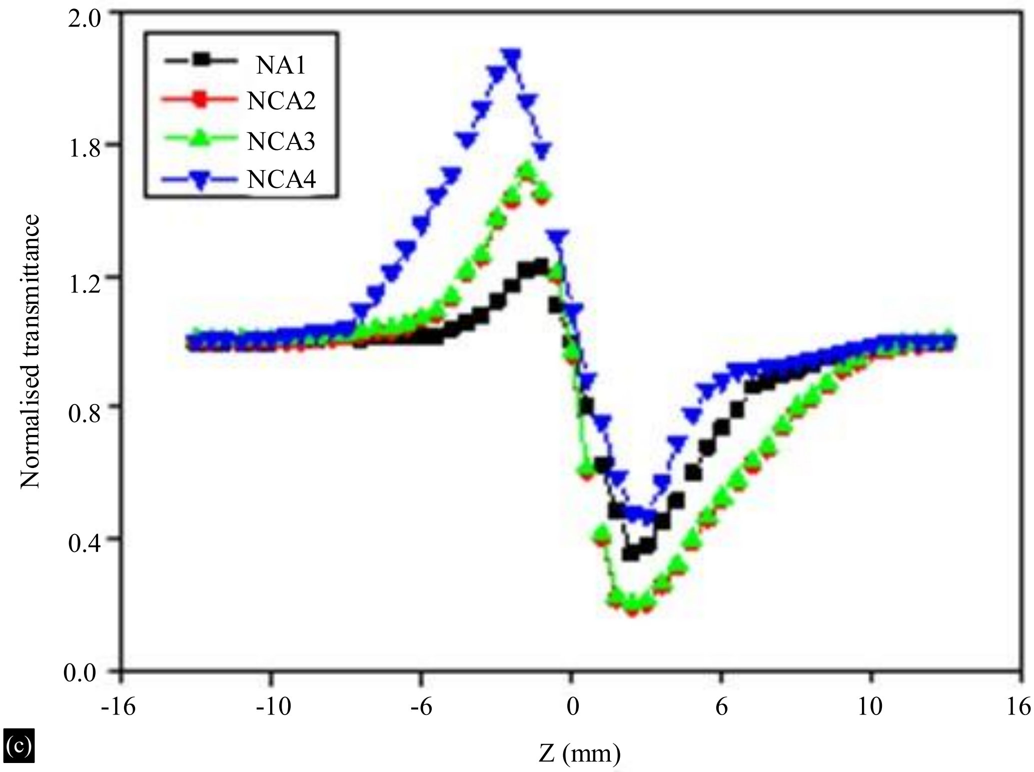

Figure 6. (a) Closed, (b) Open and (c) ratio of closed to open aperture Z-scan patterns of$Ni_{1-x}Cd_xAl_2O_4$ ($0 \leq x \leq 0.5$) nanoparticles.

The asymmetrical peak observed in the graph suggests that the material demonstrates dominance in the nonlinear absorption mechanism. Specifically, as the sample approaches the focal point, a majority of light transmits through, leading to a peak in the transmission. Beyond the focal point, there is a decline in transmission indicating saturable absorption behavior [46]. The observation of strong saturable absorption (SA) behavior, where the ground-state absorption area is larger than the excited-state absorption area upon Cd doping into the Ni aluminate system, is noteworthy [34]. The electrons of the Cd-doped Ni aluminate nanoparticles absorb the energy from the incident photons. This absorption causes the electrons to transition from lower energy levels to higher ones. The "Pauli blocking" effect refers to the phenomenon where the electrons fully occupy the higher energy states, leading to a saturation of absorption [46].

Nonlinear Refraction Measurements

The closed-aperture normalized Z-scan results depicted in Figure 6(a) provide valuable insights into the nonlinear refractive index (n_2) behavior of the synthesized materials. The characteristic of peak-valley pattern signifies a negative nonlinear refractive index (n_2) and indicative of self-defocusing behavior [47]. This means that the material acts as a triggered negative lens when exposed to continuous-wave (CW) laser radiation. The nonlinear refractive index behavior of Cd-doped Ni aluminate is influenced by both the wavelength of the exciting laser (CW 532 nm) and the composition of the sample, particularly the presence of Ni^{2+}, Cd^{2+} and Al^{3+} ions in solution dispersions.

Third-Order Nonlinearity

The Z-scan technique was effectively employed to investigate the third-order nonlinear optical properties of the synthesized Cd-doped Ni-aluminate nanoparticles. The findings are summarized in Table:3, which includes calculated and reported nonlinear properties such as the nonlinear absorption coefficient, nonlinear refractive index and the real and imaginary components of the third-order nonlinear susceptibility.

Table 3. Third order nonlinear parameters of $Ni_{1-x}Cd_xAl_2O_4$ ($0 \leq x \leq 0.5$) nanoparticles.

Sample name	Sample code	n_2 (cm²/W)	B (cm/W)	$\chi^{(3)}$ (esu)
$NiAl_2O_4$	NA1	1.91×10^{-11}	0.00523×10^{-4}	2.81×10^{-9}
$Ni_{0.9}Cd_{0.1}Al_2O_4$	NCA2	2.13×10^{-9}	0.0716×10^{-4}	6.74×10^{-7}
$Ni_{0.7}Cd_{0.3}Al_2O_4$	NCA3	3.01×10^{-9}	0.129×10^{-4}	7.12×10^{-7}
$Ni_{0.5}Cd_{0.5}Al_2O_4$	NCA4	3.47×10^{-9}	0.137×10^{-4}	7.38×10^{-6}

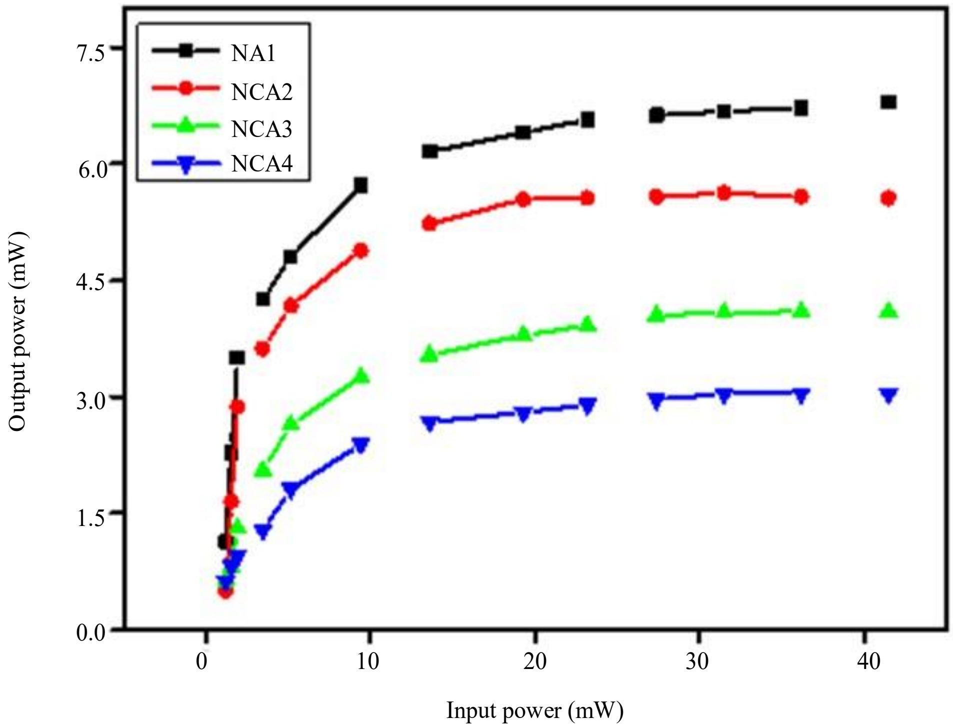

Figure 7. Optical limiting characteristics of $Ni_{1-x}Cd_xAl_2O_4$ ($0 \leq x \leq 0.5$) nanoparticles.

The samples were stimulated with a continuous-wave (CW) laser. This type of laser excitation is crucial for understanding the response of the material to a continuous and uninterrupted input, providing insights into its nonlinear optical behavior. The observed nonlinear refraction process is predominantly attributed to the thermal effects. This indicates that less laser energy is absorbed by the substance, and changes in the nonlinear refractive index are driven by thermal vibrations induced by exposure to the CW laser [48]. Thermal vibration, resulting from the local warming of the material, is responsible for the changes observed in the nonlinear refractive index. Thus, the nonlinearity in the sample associated with such thermal vibrations is due to the third-order optical nonlinearity.

Optical Limiting (OL) Studies

The continuous-wave (CW) laser for nonlinear optical studies provide valuable insights into the optical limiting behavior of Cd-doped Ni-aluminate nanoparticles. Optical limiters play a crucial role in preventing damage to optical elements, such as sensors and instruments. The use of a CW laser for nonlinear optical research allows for direct observation of the output and control of input, providing a comprehensive understanding of the materials response.

In Figure 7, the nonlinear optical response is evident as the output beam deviates from a linear relationship beyond a certain threshold amount. The power output of the beam increases with the input power, indicating the onset of optical limiting activity. The optical limiting (OL) threshold values were determined for different concentrations of Cd-doped Ni-aluminate nanoparticles. The threshold values are found to be 6.39 mW, 5.54 mW, 4.41 mW and 3.01 mW for NA1, NCA2, NCA3 and NCA4 respectively. The exceptionally high absorbance of the nonlinear substance at a specific wavelength leads to increased density and temperature in liquid samples, acting as limiting factors. The optical limitation in Cd-doped Ni-aluminate samples is attributed to a high number of defect-generated states, contributing to nonlinear absorption [49]. The defect-induced phases enhance nonlinear absorption, but also attenuate the laser intensity [50]. This enhancement in nonlinear absorption improves the nonlinear optical (NLO) characteristics of Cd-doped nickel aluminates, making them suitable for broadband optical limiting applications.

CONCLUSION

The comprehensive study on $NiAl_2O_4$ and Cd-doped $NiAl_2O_4$ nanoparticles yields remarkable information about their structural, morphological and magnetic properties that are critically relevant for advanced composite applications. In this work, Ni aluminates doped and undoped samples were synthesized using the chemical co-precipitation technique. XRD studies confirm the adoption of a cubic spinel structure with the Fd-3m space group, revealing lattice parameter values in the range between 8.0472 Å and 8.0459Å. HR-SEM images provide a detailed view of the surface morphology of the synthesized samples, offering insights into their structure and characteristics. UV-DRS spectra contribute to band gap analysis, giving values ranging from 3.51 to 4.18 eV. This information is crucial for understanding the optical properties of the materials. FT-IR wavelengths highlight the presence of functional groups in $NiAl_2O_4$ spinel nanoparticles, offering information about the bonding and chemical composition. Saturation magnetization (M_s) values for $NiAl_2O_4$ nanoparticles range from 0.51 to 1.08 emu/g, indicating the sensitivity to crystallite shape and size. Nonlinear absorption coefficient and refractive index values are of the order of 10^{-8} cm²/W and 10^{-4} cm/W, respectively, indicating a significant nonlinear effect by the samples under research. The study emphasizes the effectiveness of Cd^{2+} ion doping in nickel spinel aluminate for optical protection devices. The calculated third-order susceptibility (χ^3) and optical limiting thresholds underscore the suitability of these nanoparticles for incorporation into polymer-based optical protection devices and photonic composites. Overall, the results highlight the potential of Cd-doped $NiAl_2O_4$ as a functional nanofiller in the design of multifunctional polymer composites for next-generation photonic, optoelectronic, and magneto-optical applications.

REFERENCES

1. Shao, Zhiyu, Xiaotian Wu, et al. Synthesis and advantages of spinel-type composites. Mater. Chem. Front. 2023; 7(21): 5288-5308p.
2. Gadhwal, Reena, Ambika Devi. A review on the development of optical limiters from homogeneous to reflective 1-D photonic crystal structures. Opt. Laser Technol. 2021; 141: 107144p.
3. Ganeev, R. A. Nonlinear refraction and nonlinear absorption of various media. J. Opt. A: Pure Appl. Opt. 2005; 7(12): 717p.
4. He, Guang S., Qingdong Zheng, et al. Two-photon absorption based optical limiting and stabilization by using a CdTe quantum dot solution excited at optical communication wavelength of~ 1300nm. Appl. Phys. Lett. 2007; 90: 18p.
5. Philip, Reji, G. Ravindra Kumar, N. Sandhyarani, et al. Picosecond optical nonlinearity in monolayer-protected gold, silver, and gold-silver alloy nanoclusters. Phys. Rev. 2000; B62(19): 13160p.
6. Qu, Bin, Qiuyun Ouyang, et al. Nonlinear absorption, nonlinear scattering, and optical limiting properties of MoS_2–xZnO composite-based organic glasses. Phys. Chem. Chem. Phys. 2015; 17(8): 6036-6043p.
7. Jain, Prashant K., Xiaohua Huang, et al. Noble metals on the nanoscale: optical and photothermal properties and some applications in imaging, sensing, biology, and medicine. Acc. Chem. Res. 2008; 41(12): 1578-1586p.
8. Bansal, Vipul, Pankaj Poddar, et al. Room-temperature biosynthesis of ferroelectric barium titanate nanoparticles. J. Am. Chem. Soc. 2006; 128(36): 11958-11963p.
9. Liu, Wen-Tso. Nanoparticles and their biological and environmental applications. J. Biosci. Bioeng. 2006; 102(1): 1-7p.

10. Lang, Claus, Dirk Schüler, Damien Faivre. Synthesis of magnetite nanoparticles for bio-and nanotechnology: genetic engineering and biomimetics of bacterial magnetosomes. Macromol. Biosci. 2007; 7(2): 144-151p.
11. Chavali, Murthy S., Maria P. Nikolova. Metal oxide nanoparticles and their applications in nanotechnology. SN Appl. Sci. 2019; 1(6): 607p.
12. Ahmad, Imran, Tahir Abbas, M. U. Islam, et al. Study of cation distribution for Cu–Co nanoferrites synthesized by the sol–gel method. Cer. Inter. 2013; 39(6): 6735-6741p.
13. Belavi, P. B., G. N. Chavan, L. R. Naik, et al. Structural, electrical and magnetic properties of cadmium substituted nickel–copper ferrites. Mater. Chem. Phys. 2012; 132(1): 138-144p.
14. Xue, Jialing, Xueyi Zhang, et al. Three-dimensional flower-like $Ni_9S_8/NiAl_2O_4$ nanocomposites composed of ultra-thin porous nanosheets: Fabricated, characterized and ultra-fast NOx gas sensors at room temperature. J. Alloys Compd. 2020; 825: 154151p.
15. Mohandessi, Masoumeh, Mina Tavakolian, et al. Cadmium as a robust and novel promoter over Ni@ γ-Al_2O_3 catalysts in dry methane reforming. CS Appl. Energy Mater. 2013; 6(15): 8209-8220p.
16. Saleh, Tawfik A., Nagaraj P. Shetti, et al. Recent trends in functionalized nanoparticles loaded polymeric composites: an energy application. Mater Sci Energy Technol. 2020; 3: 515-525p.
17. Zhang, Xin, Bao-Wen Li, et al. Superior energy storage performances of polymer nanocomposites via modification of filler/polymer interfaces. Adv. Mater. Interfaces. 2018; 5(11): 1800096p.
18. Chen, Hao, Min Ling, et al. Exploring chemical, mechanical, and electrical functionalities of binders for advanced energy-storage devices. Chem. Rev. 2018; 118(18): 8936-8982p.
19. Ibiyemi, A. A., G. T. Yusuf, O. Olubosede, et al. x-ray Photoelectric and magnetic properties of chemically synthesized Cd–Ni Ferrite nanomagnetic particles. Phys. Scr. 2022; 97(2): 025804p.
20. Yuvaraj, S., S. Revathi, Anuj Kumar, et al. Impact of Cd^{2+} substituted $ZnAl_2O_4$ spinel nanoparticles on structural, optical, morphological, magnetic and nonlinear optical behaviour. Opt. Mater. 2023; 145: 114423p.
21. Gingasu, Dana, Ovidiu Oprea, et al. Structural, Morphological, and Optical Properties of Single and Mixed Ni-Co Aluminates Nanoparticles. Inorg. 2023; 11(9): 371p.
22. AL-Mamoori, Mohammed HK, Dunia K. Mahdi, et al. Synthesis and spectroscopic study of CdS nanoparticles using hydrothermal method. AIP Conf. Proc. 2018; 1968: 1p.
23. Almeshaal, Mohammed, Sivasubramanian Palanisamy, et al. Physico-chemical characterization of Grewia Monticola Sond (GMS) fibers for prospective application in biocomposites. J. Nat. Fibers. 2022; 19(17): 15276-15290p.
24. Santulli, Carlo, Sivasubramanian Palanisamy, et al. Pineapple fibers, their composites and applications. Pla. Fib., Com., and App. Woodhead Publishing; 2022: 323-346p.
25. Palanisamy, Sivasubramanian, Kalimuthu Mayandi, et al. Mechanical properties of phormium tenax reinforced natural rubber composites. Fib. 2021; 9(2): 11p.
26. Sumesh, K. R., Sivasubramanian Palanisamy, Tabrej Khan, et al. Mechanical, morphological and wear resistance of natural fiber/glass fiber-based polymer composites. BioResou. 2024;19(2): 3271-3289p.
27. Palanisamy, Sivasubramanian, Mayandi Kalimuthu, et al. Tailoring epoxy composites with Acacia caesia bark fibers: Evaluating the effects of fiber amount and length on material characteristics. Fib. 2023; 11(7): 63p.
28. Palaniappan, Murugesan, Sivasubramanian Palanisamy, et al. Novel Ficus retusa L. aerial root fiber: a sustainable alternative for synthetic fibres in polymer composites reinforcement. Bio. Conver. and Biorefin. 2025; 15(5): 7585-7601p.
29. Ranjbar, Atieh, Abdullah Irankhah, et al. Catalytic activity of rare earth and alkali metal promoted (Ce, La, Mg, K) Ni/Al_2O_3 nanocatalysts in reverse water gas shift reaction. Res. Chem. Intermed. 2019; 45: 5125-5141p.
30. Deraz, N. M. Synthesis and characterization of nano-sized nickel aluminate spinel crystals. Int. J. Electrochem. Sci. 2013; 8(4): 5203-5212p.
31. Yang, Hu, Xingxing Yang, et al. Effect of Cd2+ substitution on structural–magnetic and dielectric properties of Ni–Cu–Zn spinel ferrite nanomaterials by Sol–Gel. Molec. 2023; 28(16): 6110p.

32. Nasr, M. H., M. M. Elkholy, L. M. S. El-Deen, et al. A comprehensive study on crystal structure, magnetic, and electrical properties of Ni-doped Fe–Cd spinel nano-ferrites. J. Mater. Sci.: Mater. Electron. 2022; 33(19): 15652-15664p.
33. Ahamad, H. S., K. G. Rewatkar, N. S. Meshram, et al. Synthesis and study of Co doped Ni-Cd ferro-spinels by microwave assisted sol-gel auto-combustion method. Ferroelectr. 2020; 555(1): 146-160p.
34. Mukherjee, Indrajyoti, Gargi Dinda, et al. Synthesis, characterization, and applications of microheterogeneous-templated CdS nanodispersions. J. Nanopart. Res. 2012; 14: 1-14p.
35. Farahmandjou, Majid, Abolfazl Khodadadi, et al. Low concentration iron-doped alumina (Fe/Al_2O_3) nanoparticles using co-precipitation method. J. Supercond. Nov. Magn. 2020; 33(11): 3425-3432p.
36. Jayasree, S., A. Manikandan, S. Arul Antony, et al. Magneto-Optical and catalytic properties of Recyclable spinel $NiAl_2O_4$ Nanostructures using facile combustion methods. J. Supercond. Nov. Magn. 2016; 29: 253-263p.
37. Tangcharoen, Thanit, Jiraroj T-Thienprasert, et al. Effect of calcination temperature on structural and optical properties of MAl_2O_4 (M= Ni, Cu, Zn) aluminate spinel nanoparticles. J. Adv. Ceram. 2019; 8: 352-366p.
38. Beyranvand, Morteza, Ahmad Zahedi, et al. Cadmium substitution effect on microstructure and magnetic properties of Mg-Cu-Zn ferrites. Front. Mater. 2022; 8: 779837p.
39. Arshad, Muhammad Imran, M. S. Hasan, et al. Structural, optical, electrical, dielectric, molecular vibrational and magnetic properties of La^{3+} doped Mg–Cd–Cu ferrites prepared by Co-precipitation technique. Cer. Inter. 2022; 48(10): 14246-14260p.
40. Verma, Vivek, M. Abdullah Dar, et al. Magnetic properties of nano-crystalline $Li_{0.35}Cd_{0.3}Fe_{2.35}O_4$ ferrite prepared by modified citrate precursor method. Mater. Chem. Phys. 2010; 122(1): 133-137p.
41. Hossen MM, Nasrin S, Hossen MB. Effect of Mn^{2+} doping on structural, magnetic and electrical properties of $Ni_{0.5-x}Mn_xCu_{0.2}Cd_{0.3}Fe_2O_4$ nano ferrites prepared by sol-gel auto combustion method for high-frequency applications. Phys. B: Condens. Matter. 2020; 599: 412456p.
42. Maddahfar, Mahnaz, Majid Ramezani, et al. $NiAl_2O_4$ nanoparticles: synthesis and characterization through modify sol–gel method and its photocatalyst application. J. Mater. Sci.: Mater. Electron. 2015; 26: 7745-7750p.
43. Ati, Ali A., Zulkafli Othaman, et al. Influence of cobalt on structural and magnetic properties of nickel ferrite nanoparticles. J. Mol. Struct. 2013; 1052: 177-182p.
44. Sundararajan, M., J. Vidhya, R. Revathi, et al. Rapid synthesis and magnetic property characterization of Mg2+ doped Co3O4 nanostructures. Inorg. Nano-Metal Chem. 2022; 52(7): 996-1002p.
45. Nirmala, T. Sofia, N. Iyandurai, S. Yuvaraj, et al. Third order nonlinear optical behavior and optical limiting properties of Ni^{2+} ions doped zinc nano-aluminates. Opt. Mater. Express. 2022; 124: 111950p.
46. Yan, Lei, Mingkai Wang, et al. Enhanced and tunable nonlinear optical responses of nitrogen-doped nickel oxide induced by femtosecond laser excitation. Optic. Mater. 2020; 106: 109987p.
47. Jiménez-Pérez, J. L., R. Gutiérrez-Fuentes, G. López-Gamboa, et al. Measurement of optical nonlinear refractive index response of graphene nanoparticles dispersed in an aqueous solution by Z scan technique. Optic. Mater. 2018; 84: 236-241p.
48. Ristau, Detlev, Marco Jupé, Kai Starke. Laser damage thresholds of optical coatings. Thin Solid Films. 2009; 518(5): 1607-1613p.
49. Iliopoulos, Konstantinos, D. Kasprowicz, et al. Multifunctional $Bi_2ZnOB_2O_6$ single crystals for second and third order nonlinear optical applications. App. Phy. Let. 2013; 103: 23p.
50. Shiju, E., Siji Narendran NK, et al. Enhanced nonlinear absorption and efficient power limiting action of Au/Ag@ graphite core-shell nanostructure synthesized by laser ablation. Nano Expre. 2020; 1(3): 030026p.

